Communications in Physics, Vol. 29, No. 2 (2019), pp. 163-172
DOI:10.15625/0868-3166/29/2/13582

$\mathcal{O}(\alpha^3)$ ISR CORRECTIONS TO SINGLE HIGGS PRODUCTIONS AT FUTURE LEPTON COLLIDERS

KHIEM HONG PHAN† AND DZUNG TRI TRAN

VNUHCM-University of Science, 227 Nguyen Van Cu, Dist. 5, Ho Chi Minh City, Vietnam

†*E-mail:* phkhiem@hcmus.edu.vn

Received 23 January 2019
Accepted for publication 8 March 2019
Published 15 May 2019

Abstract. *In this paper, we present $\mathcal{O}(\alpha^3)$ QED corrections due to initial-state photon radiation (ISR) to processes $e^-e^+ \to f\bar{f}H$ with $f = e, \mu, \nu_e, \nu_\mu, \nu_\tau$ at future lepton colliders. The impact of the ISR corrections on the total cross sections is studied. We find that the corrections vary from $\sim -30\%$ to -10% in the range of center-of-mass energies ($\sqrt{s}$) from 200 GeV to 700 GeV. Moreover, the ISR corrections to some realistic distributions of experimental interest for searching the properties of the Higgs boson are evaluated numerically. They are of the order of $\sim -10\%$ contributions at $\sqrt{s} = 250$ GeV. The corrections are massive contributions and they must be taken into account for matching high-precision data at future lepton colliders.*

Keywords: Higgs boson, electron-positron colliders, QED corrections, future lepton colliders, Initial-state photon radiation.

Classification numbers: 13.66.Fg, 14.65.Ha, 14.80.Bn, 31.30.jg.

I. INTRODUCTION

The discovery of the Standard Model-like Higgs boson at the Large Hadron Collider (LHC) in 2012 [1, 2] has opened up a new era in particle physics. The research focuses on the precision measurements of the Standard Model (SM) to understand deeply the nature of this boson and searching for physics beyond the Standard Model (BSM). In particular, one of the main targets of the High-Luminosity Large Hadron Collider (HL-LHC) [3, 4] and future lepton colliders [5–10] is to measure the properties of the Higgs boson. The measurements will be performed at high precision. For example, the Higgs boson couplings will be probed at the precision of 1% or better for a statistically significant measurement [5]. In order to match the high-precision data at future

colliders, theoretical predictions including higher-order corrections to the Higgs productions are necessary.

At the electron-positron annihilation colliders, the main Higgs production channels are Higgs-strahlung processes ($e^-e^+ \to \mu^-\mu^+ H$, $\bar{\nu}_\mu \nu_\mu H$, $\bar{\nu}_\tau \nu_\tau H$) and WW-, ZZ-fusion processes ($e^-e^+ \to \bar{\nu}_e \nu_e H$, $e^-e^+ \to e^-e^+ H$ respectively). In the low-energy regions, the Higgs-strahlung processes are the dominant channels. Their cross sections increase up to the threshold (around $M_H + M_Z$) and fall off as a function of s^{-1} beyond the peak. In two latter processes, their corresponding cross sections develop as a function of $\ln s$. Thus, these channels are dominant in the high-energy regions. Recently, the advantage of the recoil mass technique [11] has been applied to extract the ZH event which is independent of the Higgs decay channels. Hence, the cross sections for these processes and their relevant distributions can be measured to few sub-percent accuracy.

Full one-loop electroweak radiative corrections to the processes $e^-e^+ \to ZH$ have been reported in [12–16]. In addition, the single Higgs productions including full one-loop electroweak corrections at lepton colliders have recently been calculated in [17–21]. However, the computations have not considered the higher-order QED corrections which are assumed to be dominant contributions at typical energy regions for the measurements of the Higgs properties. More recently, the ISR corrections to the process $e^-e^+ \to ZH \to \mu^-\mu^+ b\bar{b}$ at future lepton colliders have been presented in [22] and the corrections vary from $\sim -35\%$ to $\sim -5\%$ contributions in the range of center-of-mass energies from 200 GeV to 350 GeV.

In this work, we evaluate the $\mathcal{O}(\alpha^3)$ QED corrections due to the initial-state photon radiation to the processes $e^-e^+ \to f\bar{f}H$ with $f = e, \mu, \nu_e, \nu_\mu, \nu_\tau$ at future lepton colliders. We then study the effects of the ISR corrections on the total cross section and its relevant distributions. Our paper is organised as follows: In the next section, we present the calculation in detail. In section *III*, we discuss on the numerical results for the processes at future colliders. Finally, conclusions and future prospects will be devoted in section *IV*.

II. THE CALCULATIONS

Following the factorization theorems, the total cross section for single Higgs productions including the initial-state QED corrections can be expressed as a convolution of the two structure functions (SF) for two beams and of the lowest-order cross section as follows:

$$\sigma(s) = \int dx_1 dx_2 D(x_1, Q^2) D(x_2, Q^2) \hat{\sigma}_0(x_1 x_2 s), \tag{1}$$

where $\hat{\sigma}_0(x_1 x_2 s)$ is tree-level cross section for the processes $e^-e^+ \to f\bar{f}H$ with $f = e, \mu, \nu_e, \nu_\mu, \nu_\tau$. It is computed at the reduced center-of-mass energy $\hat{s} = x_1 x_2 s$. In Eq. (1), $D(x, Q^2)$ is the non-singlet collinear SF for modeling the initial-state photon radiation at the energy scale Q^2. This function explains for the probability to find an electron possessing momentum fraction x at the energy scale Q^2 inside an electron parent. The SF applied in this work is written as follows:

$$D_{GL}(x, Q^2) = \frac{\exp\left[\frac{1}{2}\beta\left(\frac{3}{4} - \gamma_E\right)\right]}{\Gamma\left(1 + \frac{1}{2}\beta\right)} \frac{1}{2}\beta\,(1-x)^{\frac{1}{2}\beta - 1}, \tag{2}$$

where

$$\beta = \frac{2\alpha}{\pi}(L-1), \qquad L = \ln(Q^2/m_e^2). \tag{3}$$

Here, α is the fine structure constant, m_e is the electron mass, Γ is the Gamma function, γ_E is Euler-Mascheroni constant. In this work, both additive and factorized structure functions are applied for modeling the ISR corrections. The additive SF up to third finite order reads [23]:

$$
\begin{aligned}
D_A(x,Q^2) =& \sum_{i=0}^{3} d_A^{(i)}(x,Q^2),\\
d_A^{(0)}(x,Q^2) =& D_{GL}(x,Q^2),\\
d_A^{(1)}(x,Q^2) =& -\frac{1}{4}\beta(1+x),\\
d_A^{(2)}(x,Q^2) =& \frac{1}{32}\beta^2\left[(1+x)\left(-4\ln(1-x)+3\ln(x)\right)-4\frac{\ln x}{1-x}-5-x\right],\\
d_A^{(3)}(x,Q^2) =& \frac{1}{384}\beta^3\Bigg\{(1+x)\left[18\zeta(2)-6\mathrm{Li}_2(x)-12\ln^2(1-x)\right]\\
&+\frac{1}{1-x}\left[-\frac{3}{2}(1+8x+3x^2)\ln x-6(x+5)(1-x)\ln(1-x)\right.\\
&-12(1+x^2)\ln x\ln(1-x)+\frac{1}{2}(1+7x^2)\ln^2 x\\
&\left.-\frac{1}{4}(39-24x-15x^2)\right]\Bigg\}.
\end{aligned}
\tag{4}
$$

where ζ is the Riemann zeta-function and Li_2 is the dilogarithm function.

Furthermore, the factorized SF given up to third order finite terms can be found in [24, 25] whose formulas are expressed as follows:

$$
\begin{aligned}
D_F(x,Q^2) =& D_{GL}(x,Q^2)\sum_{i=1}^{3} d_F^{(i)}\\
d_F^{(1)}(x,Q^2) =& \frac{1}{2}(1+x^2),\\
d_F^{(2)}(x,Q^2) =& \frac{1}{4}\frac{\beta}{2}\left[-\frac{1}{2}(1+3x^2)\ln x-(1-x)^2\right],\\
d_F^{(3)}(x,Q^2) =& \frac{1}{8}\left(\frac{\beta}{2}\right)^2\left[(1-x)^2+\frac{1}{2}(3x^2-4x+1)\ln x\right.\\
&\left.+\frac{1}{12}(1+7x^2)\ln^2 x+(1-x^2)\mathrm{Li}_2(1-x)\right].
\end{aligned}
\tag{5}
$$

The above functions are valid in the soft photon limit. The additive SF has been derived as Gribov-Lipatov solution.

At tree level, we have 21, 42 and 12 Feynman diagrams for the processes $e^-e^+ \to \mu^-\mu^+H$, e^-e^+H and $\nu_e\bar{\nu}_eH$ respectively. In Fig. 1, we show several typical Feynman diagrams for $e^-e^+ \to \mu^-\mu^+H$.

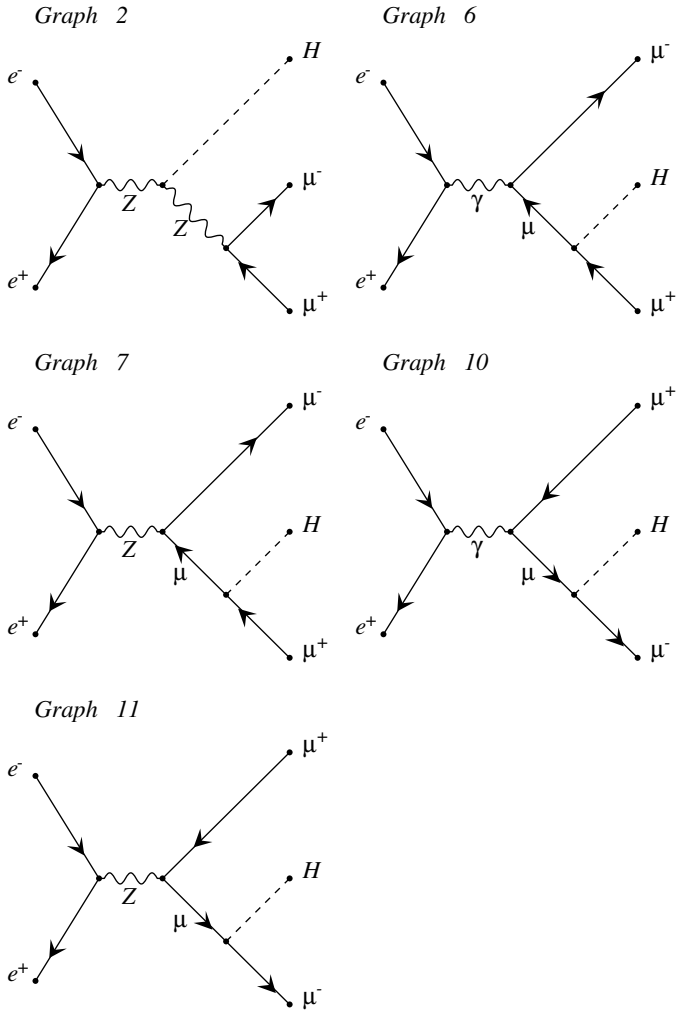

Fig. 1. Typical Feynman diagrams for the process $e^-e^+ \to \mu^-\mu^+H$.

In this calculation, the tree level cross sections are generated by using GRACE program [27]. GRACE program provides the internal numerical checks for the calculation, e.g., test of gauge invariance. Furthermore, the cross sections of the processes $e^-e^+ \to f\bar{f}H$ at lowest-order diagrams are also checked with other programs. For example, in Appendix 1, we cross-check this work with [19] at lowest-order of the processes $e^-e^+ \to \nu_f\bar{\nu}_fH$. We find that our results are in good agreement with [19]. After checking successfully the generated codes, we are going to discuss the numerical results with including the $\mathcal{O}(\alpha^3)$ ISR corrections to these reactions at future lepton colliders.

III. NUMERICAL RESULTS

We use the following input parameters for the calculation: the fine structure constant in the Thomson limit is $\alpha^{-1}(Q^2 \to 0) = 137.0359895$. The mass of the Higgs boson is $M_H = 126$ GeV and the Z boson mass is $M_Z = 91.1876$ GeV. Because of the limited accuracy of the measured value for M_W, we hence take the value that is derived from the electroweak radiative corrections to the muon decay width (Δr) [28] with $G_F = 1.16639 \times 10^{-5}$ GeV^{-2}. As a result, M_W is a function of M_H. The resulting $M_W = 80.370$ GeV is corresponding to $\Delta r = 2.49\%$. Finally, for the lepton masses we take $m_e = 0.51099891$ MeV, $m_\mu = 105.658367$ MeV and $m_\tau = 1776.82$ MeV. For the quark masses, we take $m_u = 63$ MeV, $m_d = 63$ MeV, $m_c = 1.5$ GeV, $m_s = 94$ MeV, $m_t = 173.5$ GeV, and $m_b = 4.7$ GeV.

In this work, the QED corrections are evaluated in the so-called "$\alpha(0)$" scheme. Since the running coupling constant $\alpha(Q^2)$ from Thompson value to the scale $Q^2 = s$ (the center-of-mass energy s) will take into account the leading contributions which are from vacuum polarization and they can be treated as pure weak corrections [26]. As a matter of fact, we take $\alpha(Q^2)$ fixed at the Thomson value in this work. To study the impact of the QED corrections, we define the correction factor as follows:

$$K_{\rm QED} = \frac{\sigma_{\mathscr{O}(\alpha^3)} - \sigma_0}{\sigma_0}. \tag{6}$$

We are going to discuss the numerical results for these reactions in the following paragraphs. We first arrive at the results for the process $e^-e^+ \to \mu^-\mu^+H$. In Fig. 2(a), the total cross section with including the $\mathscr{O}(\alpha^3)$ ISR corrections are presented as a function of center-of-mass energy $\sqrt{s}$. The $\sqrt{s}$ varies from 200 GeV to 700 GeV. In this Figure, the black solid-line presents for tree level cross section for this process (without the ISR corrections). The blue (and red) solid-line is shown for the $\mathscr{O}(\alpha^3)$ ISR corrections. We find that the cross section increases up to the peak at the threshold (around 250 GeV). It then decreases similar to the function of s^{-1} beyond the peak. The $K_{\rm QED}$ factor presented for the ISR corrections, is shown in the right top corner of this Figure. We observe that the corrections are range of $\sim -30\%$ to $\sim -10\%$ contributions to the total cross sections. The large QED corrections around the threshold are attributed for Coulomb effects [29,30]. Both the ISR corrections corresponding to the structure functions in Eq. (4) and in Eq. (5) are used for modeling the QED corrections. They give the same results within Monte Carlo errors at low-energy regions and they are different about few percent at high-energy regions. The discrepancy may be attributed to higher order corrections ($\mathscr{O}(\alpha^4)$). This topic will be discussed in future publication.

The differential cross sections are shown as functions of the energy of muon, the invariant mass of $\mu^-\mu^+$ and the rapidity of muon at $\sqrt{s} = 250$ GeV. In Figs. 2(b,c,d), one presents the differential cross section without the ISR corrections as black solid-line. The blue (and red) solid-line is corresponding to the ISR corrections. In Fig. 2(b), the distribution of cross section as a function of E_μ (muon's energy) at $\sqrt{s} = 250$ GeV is discussed. The corrections change from $\sim -30\%$ to $\sim -15\%$ in the range of E_μ from 10 GeV to 70 GeV. We observe a peak of Z boson mass which decays to muon pair at ~ 90 GeV in Fig. 2(c). One finds that the QED corrections are range from $\sim -15\%$ to $\sim -20\%$ in this distribution. Finally, we are interested in the rapidity distribution of muon, seen in Fig. 2(d). The ISR corrections amount to the contribution of $\sim -20\%$ in the range of $|\eta_\mu| < 2.5$.

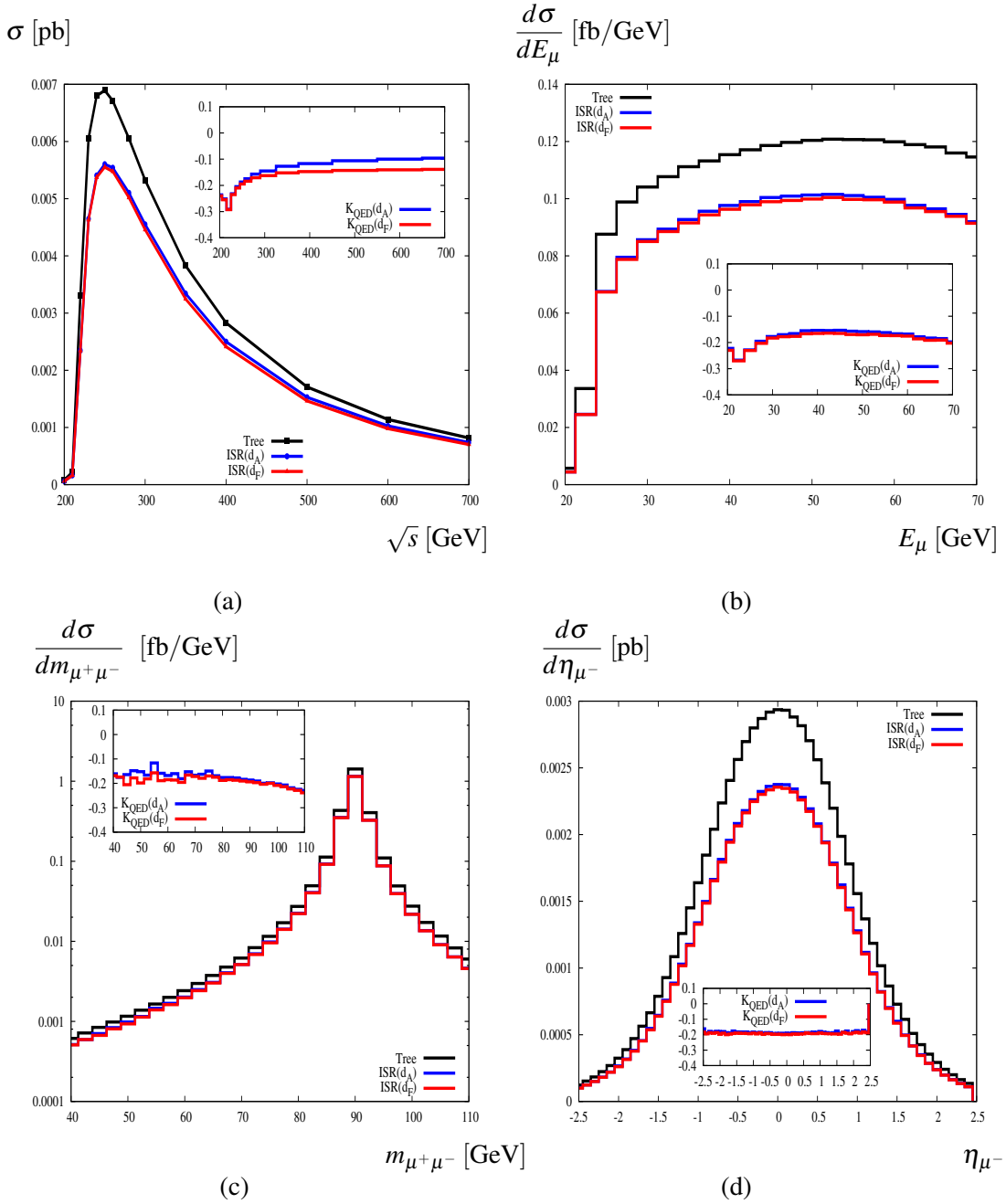

Fig. 2. Total cross sections (a), the differential cross-section as a function of the energy of muon (b), the invariant mass of μ^- and μ^+ (c) and the rapidity of muon (d). All of them are presented with the $\mathcal{O}(\alpha^3)$ ISR corrections.

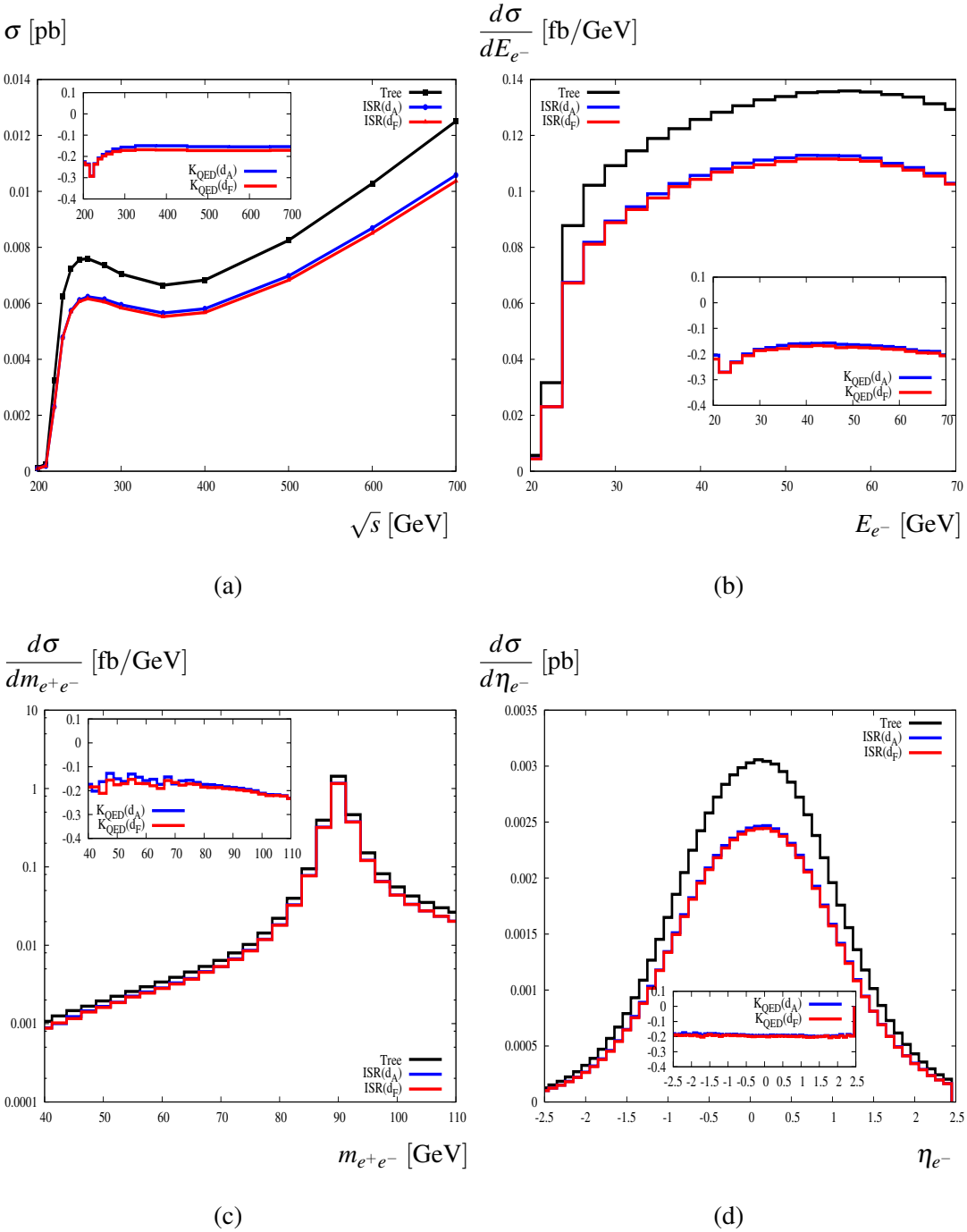

Fig. 3. Total cross sections (a), the differential cross-section as a function of the energy of electron (b), the invariant mass of e^- and e^+ (c) and the rapidity of electron (d). All of them are presented with the ISR $\mathcal{O}(\alpha^3)$ corrections.

We next turn our attention to the numerical results for the process $e^-e^+ \to e^-e^+H$. In Fig. 3(a), the total cross section including the $\mathcal{O}(\alpha^3)$ ISR corrections is presented as a function of center-of-mass energy. We find that cross section has peak at the threshold (around $M_Z + M_H$). It then increases similar to the function of $\ln s$ beyond the peak. This is explained as the dominant contributions from t-channel diagrams. These corrections are in the range of $\sim -30\%$ to $\sim -15\%$ contributions. The large corrections obtained around the threshold are also explained as the Coulomb effects. The differential cross sections as functions of the energy of electron, the invariant mass of e^-, e^+ and rapidity of electron at $\sqrt{s} = 250$ GeV are shown in Figs. 3(b,c,d). From these Figures, we observe that the QED corrections are about $\sim -30\%$ to $\sim -20\%$ contributions.

We finally change to the numerical results for the process $e^-e^+ \to \nu_f \bar{\nu}_f H$ with $f = e, \mu, \tau$. The cross sections for these processes are summed of three neutrino species. In Fig. 4, the total cross section with taking into account the $\mathcal{O}(\alpha^3)$ ISR corrections are presented as a function of center-of-mass energy. As same as the process $e^-e^+ \to e^-e^+H$, it can be seen the peak of the cross section at the threshold (around $M_Z + M_H$). It then develops similar to the function of $\ln s$ beyond the peak. The ISR corrections are in the range of $\sim -30\%$ to $\sim -15\%$. The differential cross sections as functions of the invariant mass of $\nu_f \bar{\nu}_f$ at $\sqrt{s} = 250$ GeV are displayed in Fig. 4(b). We find a peak of Z boson mass at ~ 90 GeV. The ISR corrections vary from $\sim -15\%$ to $\sim -25\%$ contributions to the differential cross sections.

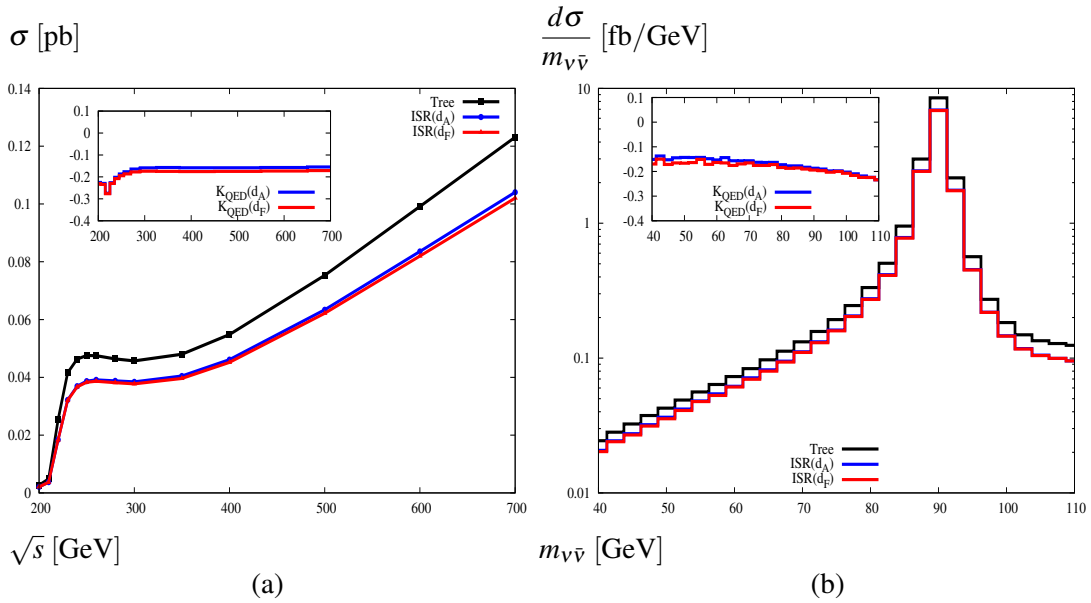

Fig. 4. Total cross section (a), differential cross-section as a function of the invariant mass of $\nu_e \bar{\nu}_e$ (b). All of them are presented with the $\mathcal{O}(\alpha^3)$ ISR corrections.

It is noted that all the invariant mass distributions presented in this section are plotted in a logarithmic scale. Other distributions are shown in a linear scale. We observe the massive contribution of the ISR corrections to the total cross sections as well as their relevant distributions. It is clear that the contributions play an important role for measuring the properties of the Higgs boson. They must be taken into account at future lepton colliders.

IV. CONCLUSIONS

We have presented the QED $\mathcal{O}(\alpha^3)$ corrections to the processes $e^-e^+ \to f\bar{f}H$ with $f = e, \mu, \nu_e, \nu_\mu, \nu_\tau$ due to the initial-state photon radiation at future lepton colliders. In this study, we have investigated the effect of the ISR corrections on the total cross section and its relevant distributions. We have found that the corrections are order of $\sim -10\%$ contributions. The corrections are massive contributions which must be taken into account for measuring the properties of the Higgs boson at future lepton colliders.

ACKNOWLEDGMENT

This research is funded by Vietnam's National Foundation for Science and Technology Development (NAFOSTED) under grant number 103.01-2016.33.

REFERENCES

[1] G. Aad *et al.* [ATLAS Collaboration], *Phys. Lett. B* **716** (2012) 1.
[2] S. Chatrchyan *et al.* [CMS Collaboration], *Phys. Lett. B* **716** (2012) 30.
[3] ATLAS Collaboration, arXiv:1307.7292 [hep-ex].
[4] CMS Collaboration, arXiv:1307.7135.
[5] H. Baer *et al.*, arXiv:1306.6352 [hep-ph].
[6] K. Fujii *et al.*, arXiv:1710.07621 [hep-ex].
[7] S. Asai *et al.*, arXiv:1710.08639 [hep-ex].
[8] CEPC-SPPC Study Group, IHEP-CEPC-DR-2015-01, IHEP-TH-2015-01, IHEP-EP-2015-01.
[9] M. Bicer *et al.* [TLEP Design Study Working Group], *JHEP* **1401** (2014) 164.
[10] M. J. Boland *et al.* [CLIC and CLICdp Collaborations], arXiv:1608.07537 [physics.acc-ph].
[11] J. Yan, S. Watanuki, K. Fujii, A. Ishikawa, D. Jeans, J. Strube, J. Tian and H. Yamamoto, *Phys. Rev. D* **94** (2016) no.11, 113002.
[12] J. Fleischer and F. Jegerlehner, *Nucl. Phys. B* **216** (1983) 469.
[13] B. A. Kniehl, *Z. Phys. C* **55** (1992) 605.
[14] A. Denner, J. Kublbeck, R. Mertig and M. Bohm, *Z. Phys. C* **56** (1992) 261.
[15] Y. Gong, Z. Li, X. Xu, L. L. Yang and X. Zhao, *Phys. Rev. D* **95** (2017) no.9, 093003.
[16] Q. F. Sun, F. Feng, Y. Jia and W. L. Sang, *Phys. Rev. D* **96** (2017) no.5, 051301.
[17] G. Belanger, F. Boudjema, J. Fujimoto, T. Ishikawa, T. Kaneko, K. Kato and Y. Shimizu, *Phys. Lett. B* **559** (2003) 252.
[18] G. Belanger, F. Boudjema, J. Fujimoto, T. Ishikawa, T. Kaneko, K. Kato, Y. Shimizu and Y. Yasui, *Phys. Lett. B* **571** (2003) 163.
[19] A. Denner, S. Dittmaier, M. Roth and M. M. Weber, *Nucl. Phys. B* **660** (2003) 289.
[20] A. Denner, S. Dittmaier, M. Roth and M. M. Weber, *Phys. Lett. B* **560** (2003) 196.
[21] A. Denner, S. Dittmaier, M. Roth and M. M. Weber, *Eur. Phys. J. C* **33** (2004) S635.
[22] M. Greco, G. Montagna, O. Nicrosini, F. Piccinini and G. Volpi, *Phys. Lett. B* **777** (2018) 294.
[23] M. Cacciari, A. Deandrea, G. Montagna and O. Nicrosini, *Europhys. Lett.* **17** (1992) 123.
[24] M. Skrzypek and S. Jadach, *Z. Phys. C* **49** (1991) 577.
[25] M. Skrzypek, *Acta Phys. Polon. B* **23** (1992) 135.
[26] M. Consoli and W. Hollik, in *Z. Physics at LEP 1*, CERN Yellow Report 89-08, edited by G. Altarelli, R. Kleiss and C. Verzegnassi (Geneva) 1989.
[27] T. Ishikawa, T. Kaneko, K. Kato, S. Kawabata, Y. Shimizu and H. Tanaka, `KEK Report 92-19, 1993, GRACE manual Ver. 1.0.`
[28] Z. Hioki, *Acta Phys. Polon. B* **27** (1996) 2573.
[29] V. S. Fadin, V. A. Khoze, A. D. Martin and A. Chapovsky, *Phys. Rev. D* **52** (1995) 1377.
[30] V. S. Fadin, V. A. Khoze, A. D. Martin and W. J. Stirling, *Phys. Lett. B* **363** (1995) 112.

APPENDIX

In this Appendix, we cross-check our results at lowest order for $e^-e^+ \to \nu_f \bar{\nu}_f H$ ($f = e, \mu, \tau$) with [19]. We take input parameters in [19] where the Higgs masses vary from 150 GeV to 350 GeV. The "$\alpha(0)$" scheme is used for this check. In this Table, the third column presents for the

Table 1. Total cross section in lowest order for $\sqrt{s} = 500$ GeV and various Higgs masses.

M_H (GeV)	M_W (GeV)	[19] (fb)	This work (fb)
150	80.3767	61.074(7)	61.07(3)
200	80.3571	37.294(4)	37.28(5)
250	80.3411	21.135(2)	21.14(1)
300	80.3275	10.758(1)	10.75(9)
350	80.3158	4.6079(5)	4.608(1)

results which are taken from [19] and the last column shows our results. We find that two results are in good agreement for all Higgs masses under consideration.